ACADEMIC PRESS

Available at www.ComputerScienceWeb.com
POWERED BY SCIENCE DIRECT®

Computer Vision and Image Understanding 91 (2003) 214–245

Computer Vision and Image Understanding

www.elsevier.com/locate/cviu

Probabilistic recognition of human faces from video ☆

Shaohua Zhou,* Volker Krueger, and Rama Chellappa

Center for Automation Research (CfAR), Department of Electrical and Computer Engineering, University of Maryland, College Park, MD 20742, USA

Received 15 February 2002; accepted 11 February 2003

Abstract

Recognition of human faces using a gallery of still or video images and a probe set of videos is systematically investigated using a probabilistic framework. In *still-to-video* recognition, where the gallery consists of still images, a time series state space model is proposed to fuse temporal information in a probe video, which simultaneously characterizes the kinematics and identity using a *motion vector* and an *identity variable*, respectively. The joint posterior distribution of the motion vector and the identity variable is estimated at each time instant and then propagated to the next time instant. *Marginalization* over the motion vector yields a robust estimate of the posterior distribution of the identity variable. A computationally efficient *sequential importance sampling* (SIS) algorithm is developed to estimate the posterior distribution. Empirical results demonstrate that, due to the propagation of the identity variable over time, a *degeneracy* in posterior probability of the identity variable is achieved to give improved recognition. The gallery is generalized to videos in order to realize *video-to-video* recognition. An *exemplar-based learning* strategy is adopted to automatically select video representatives from the gallery, serving as mixture centers in an updated likelihood measure. The SIS algorithm is applied to approximate the posterior distribution of the motion vector, the identity variable, and the exemplar index, whose marginal distribution of the identity variable produces the recognition result. The model formulation is very general and it allows a variety of image representations and transformations. Experimental results using images/videos collected at UMD, NIST/USF, and CMU with pose/illumination variations illustrate the

☆ This work was completed with the support of the DARPA HumanID Grant N00014-00-1-0908. All correspondences are addressed to rama@cfar.umd.edu. Tel: 301-405-4526. Fax: 301-314-9115. Krueger was affiliated with CfAR. He is now at the Aalborg University, Denmark.

* Corresponding author.

E-mail addresses: shaohua@cfar.umd.edu (S. Zhou), vok@cfar.umd.edu (V. Krueger), rama@cfar.umd.edu (R. Chellappa).

1077-3142/$ - see front matter
doi:10.1016/S1077-3142(03)00080-8

effectiveness of this approach for both still-to-video and video-to-video scenarios with appropriate model choices.

Keywords: Face recognition; Still-to-video; Video-to-video; Time series state space model; Sequential importance sampling; Exemplar-based learning

1. Introduction

Probabilistic video analysis has recently gained significant attention in the computer vision community since the seminal work of Isard and Blake [1]. In their effort to solve the problem of visual tracking, they introduced a time series state space model parameterized by a tracking motion vector (e.g., affine transformation parameters), denoted by θ_t. The CONDENSATION algorithm was developed to provide a numerical approximation to the posterior distribution of the motion vector at time t given the observations up to t, i.e., $p(\theta_t|z_{0:t})$ where $z_{0:t} = (z_0, z_1, \ldots, z_t)$ and z_t is the observation at time t, and to propagate it over time according to the kinematics. The CONDENSATION algorithm, also known as the particle filter (PF), was originally proposed in [2] in the signal processing literature and has been used to solve many other vision tasks [3,4], including human face recognition (FR) [5]. In this paper, we will systematically investigate the incorporation of temporal information in a video sequence for face recognition.

Face recognition has been an extensive research area for a long time. Refer to [6,7] for surveys and [8] for reports on experiments. Experiments reported in [8] evaluate *still-to-still* scenarios, where the gallery and the probe set consist of still facial images. Some well-known still-to-still FR approaches include Principal Component Analysis (PCA) [9], Linear Discriminant Analysis (LDA) [10,11], and Elastic Graph Matching (EGM)[12]. Typically, recognition is performed based on an abstract representation of the face image after suitable geometric and photometric transformations and corrections.

Following [8], we define a *still-to-video* scenario: the gallery consists of still facial templates and the probe set consists of video sequences containing the facial region. Denote the gallery as $\mathcal{I} = \{I_1, I_2, \ldots, I_N\}$, indexed by the identity variable n, which lies in a finite sample space $\mathcal{N} = \{1, 2, \ldots, N\}$. Though significant research has been conducted on still-to-still recognition, research efforts on still-to-video recognition, are relatively fewer due to the following challenges [7] in typical surveillance applications: poor video quality, significant illumination and pose variations, and low image resolution. Most existing video-based recognition systems [13] attempt the following: the face is first detected and then tracked over time. Only when a frame satisfying certain criteria (size and pose) is acquired, recognition is performed using still-to-still recognition technique. For this, the face part is cropped from the frame and transformed or registered using appropriate transformations. This *tracking-then-recognition* approach attempts to resolve uncertainties in tracking and recognition *sequentially and separately*.

There are several unresolved issues in the *tracking-then-recognition* approach: criteria for selecting good frames and estimation of parameters for registration. Also, still-to-still recognition does not effectively exploit temporal information. A common strategy that selects several good frames, performs recognition on each frame and then votes on these recognition results for a final solution might be ad hoc.

To overcome these difficulties, we propose a *tracking-and-recognition* approach, which attempts to resolve uncertainties in tracking and recognition *simultaneously* in a unified probabilistic framework. To fuse temporal information, the time series state space model is adopted to characterize the evolving kinematics and identity in the probe video. Three basic components of the model are:

- a *motion equation* governing the kinematic behavior of the tracking motion vector,
- an *identity equation* governing the temporal evolution of the identity variable,
- an *observation equation* establishing a link between the motion vector and the identity variable.

Using the sequential importance sampling (SIS) [1,14–16] technique, the joint posterior distribution of the motion vector and the identity variable, i.e., $p(n_t, \theta_t|z_{0:t})$ is estimated at each time instant and then propagated to the next time instant governed by motion and identity equations. The marginal distribution of the identity variable, i.e., $p(n_t|z_{0:t})$, is estimated to provide a recognition result. An SIS algorithm is developed to approximate the distribution $p(n_t|z_{0:t})$ in the still-to-video scenario. It achieves computational efficiency over its CONDENSATION counterpart by considering the discrete nature of the identity variable.

The still templates in the gallery can be generalized to video sequences in order to realize *video-to-video* recognition. In video-to-video recognition, exemplars and their prior probabilities are learned from the gallery videos to serve as still templates in the still-to-video scenario. A person n may have a collection of several exemplars, say $\mathcal{C}^n = \{c_1^n, c_2^n, \ldots, c_{K_n}^n\}$ indexed by k. The likelihood is modified as a mixture density with exemplars as mixture centers. We first compute the joint distribution $p(n_t, k_t, \theta_t|z_{0:t})$ using the SIS algorithm and marginalize it to yield $p(n_t|z_{0:t})$. In the experiments reported, the subject walks on a tread-mill with his/her face moving naturally, giving rise to significant variations across poses. However, the proposed method successfully cope with these pose variations as evidenced by the experimental results.

It is worth emphasizing that (i) our model can take advantage of any still-to-still recognition algorithm [9–12] by embedding distance measures used therein in our likelihood measurement and (ii) it allows a variety of image representations and transformations.

The organization of the paper is as follows: Section 2 reviews some related studies on (i) face modeling and recognition and (ii) video-based tracking and recognition in the literature. Section 3 introduces the time series state space model for recognition and establishes the time-evolving behavior of $p(n_t|z_{0:t})$. Section 4 briefly reviews the SIS principles from the viewpoint of a general state space model and develops a SIS algorithm to solve the still-to-video recognition problem, with a special emphasis on

its computational efficiency. Section 5 describes the experimental scenarios for still-to-video recognition and presents results using data collected at UMD, NIST/USF, and CMU (MoBo database) as part of the HumanID effort. In Section 6, the exemplar-based learning algorithm and the SIS algorithm to accommodate video-to-video recognition are presented. Experimental results for video-to-video recognition problem using the CMU data are also included in this section. Section 7 concludes the paper with discussions.

2. Related literature

2.1. Face modeling and recognition

Statistical approaches to face modeling have been very popular since Turk and Pentland's work on eigenface in 1991 [9]. In statistical approach, the two-dimensional appearance of face image is treated as a vector by scanning the image in lexicographical order, with the vector dimension being the number of pixels in the image. In the eigenface approach [9], all face images consists of a distinctive face subspace. This subspace is linear and spanned by the eigenvectors of the covariance matrix found using PCA. Typically we keep the number of eigenvectors much less than the true dimension of the vector space. The task of face recognition is then to find the closest match in this face subspace. However, PCA might not be efficient in terms of recognition accuracy since the construction of the face subspace does not capture discrimination between humans. This motivates the use of LDA [11,10] and its variants. In LDA, the linear subspace is constructed [17] in such a manner that the within-class scatter is minimized and the between-class scatter is maximized. This idea is further generalized in the approach called Bayesian face recognition [18], where intra-personal space (IPS) and extra-personal space (EPS) are used in lieu of within-class scatter and between-class scatter measures. The IPS models the variations in the appearance of the same individual and the EPS models the variations in the appearance due to a difference in the identity. Probabilistic subspace density is then fitted on each space. A Bayesian decision is taken using a *maximum a posteriori* (MAP) rule to determine the identity.

Neural-networks have also been commonly used for face recognition. In the famous EGM [12] algorithm, the face is represented as a labeled graph, where each node is labeled with jets derived from responses obtained by convolving the image with a family of Gabor functions. The edge characterizes the geometric distance between two nodes. Face recognition is then formalized as a graph matching problem.

All the above approaches are based on 2D appearance and perform poorly when significant pose and illumination variations are present [8]. To completely resolve such challenges, 3D face modeling [19] is necessary. However, building a 3D face model is a very difficult and complicated task in the literature even though structure from motion has been studied for several decades.

2.2. Video-based tracking and recognition

Nearly all video-based recognition systems apply still-image-based recognition to selected good frames. The face images are warped into frontal views whenever pose and depth information about the faces is available [13].

In [20–22], Radial Basis Function (RBF) networks are used for tracking and recognition purposes. In [20], the system uses an RBF network for recognition. Since no warping is done, the RBF network has to learn the individual variations as well as possible transformations. The performance appears to vary widely, depending on the size of the training data. [22] presents a fully automatic person authentication system. The system uses video break, face detection, and authentication modules and cycles over successive video images until a high recognition confidence is reached. This system was tested on three image sequences; the first was taken indoors with one subject present, the second was taken outdoors with two subjects, and the third was taken outdoors with one subject in stormy conditions. Perfect results were reported on all three sequences, when verified against a database of 20 still face images.

In [23], a system called *PersonSpotter* is described. This system is able to capture, track and recognize a person walking toward or passing a stereo CCD camera. It has several modules, including a head tracker, and a landmark finder. The landmark finder uses a dense graph consisting of 48 nodes learned from 25 example images to find landmarks such as eyes and nose tip. An elastic graph matching scheme is employed to identify the face.

A multimodal based person recognition system is described in [13]. This system consists of a face recognition module, a speaker identification module, and a classifier fusion module. The most reliable video frames and audio clips are selected for recognition. 3D information about the head is used to detect the presence of an actual person as opposed to an image of that person. Recognition and verification rates of 100% were achieved for 26 registered clients.

In [24], recognition of face over time is implemented by constructing a face identity surface. The face is first warped to a frontal view, and its Kernel Discriminant Analysis (KDA) features over time form a trajectory. It is shown that the trajectory distances accumulate recognition evidence over time.

In [5], a generic approach to simultaneous object tracking and verification is proposed. The approach is based on posterior probability density estimation using sequential Monte Carlo methods [1,14–16]. Tracking is formulated as a probability density propagation problem and the algorithm also provides verification results. However, no systematic evaluation of recognition was done. Our approach looks similar to this algorithm; however, there are significant differences from the algorithm described in [5]. We highlight the differences in Section 7.

3. A model for recognition in video

In this section, we present the details on the propagation model for recognition and discuss its impact on the posterior distribution of identity variable.

3.1. A time series state space model for recognition

3.1.1. Motion equation

In its most general form, the motion model can be written as

$$\theta_t = g(\theta_{t-1}, u_t);\ t \geqslant 1, \tag{1}$$

where u_t is *noise* in the motion model, whose distribution determines the motion state transition probability $p(\theta_t|\theta_{t-1})$. The function $g(\cdot,\cdot)$ characterizes the evolving motion and it could be a function learned offline or given a priori. One of the simplest choice is an additive function, i.e., $\theta_t = \theta_{t-1} + u_t$, which leads to a first-order Markov chain.

Choice of θ_t is application dependent. Affine motion parameters are often used when there is no significant pose variation available in the video sequence. However, if a 3D face model is used, 3D motion parameters should be used accordingly.

3.1.2. Identity equation

$$n_t = n_{t-1};\ t \geqslant 1, \tag{2}$$

assuming that the identity does not change as time proceeds.

3.1.3. Observation equation

By assuming that the transformed observation is a noise-corrupted version of some still template in the gallery, the observation equation can be written as

$$\mathcal{T}_{\theta_t}\{z_t\} = I_{n_t} + v_t;\ t \geqslant 1, \tag{3}$$

where v_t is *observation noise* at time t, whose distribution determines the observation likelihood $p(z_t|n_t,\theta_t)$, and $\mathcal{T}_{\theta_t}\{z_t\}$ is a transformed version of the observation z_t. This transformation could be either geometric or photometric or both. However, when confronting sophisticated scenarios, this model is far from sufficient. One should seek for complicated likelihood measurement as shown in Section 5.

We assume statistical independence between all noise variables and prior knowledge on the distributions $p(\theta_0|z_0)$ and $p(n_0|z_0)$. Using the overall state vector $x_t = (n_t, \theta_t)$, Eqs. (1) and (2) can be combined into one state equation (in a normal sense) which is completely described by the overall state transition probability

$$p(x_t|x_{t-1}) = p(n_t|n_{t-1})p(\theta_t|\theta_{t-1}). \tag{4}$$

Given this model, our goal is to compute the posterior probability $p(n_t|z_{0:t})$. It is in fact a probability mass function (PMF) since n_t only takes values from $\mathcal{N} = \{1, 2, \ldots, N\}$, as well as a marginal probability of $p(n_t, \theta_t|z_{0:t})$, which is a mixed distribution. Therefore, the problem is reduced to computing the posterior probability.

3.2. The posterior probability of identity variable

The evolution of the posterior probability $p(n_t|z_{0:t})$ as time proceeds is very interesting to study as the identity variable does not change by assumption, i.e., $p(n_t|n_{t-1}) = \delta(n_t - n_{t-1})$, where $\delta(\cdot)$ is a discrete impulse function at zero.

Using time recursion, Markov properties, and statistical independence embedded in the model, we can easily derive:

$$\begin{aligned} p(n_{0:t}, \theta_{0:t}|z_{0:t}) &= p(n_{0:t-1}, \theta_{0:t-1}|z_{0:t-1}) \frac{p(z_t|n_t, \theta_t)p(n_t|n_{t-1})p(\theta_t|\theta_{t-1})}{p(z_t|z_{0:t-1})} \\ &= p(n_0, \theta_0|z_0) \prod_{s=1}^{t} \frac{p(z_s|n_s, \theta_s)p(n_s|n_{s-1})p(\theta_s|\theta_{s-1})}{p(z_s|z_{0:s-1})} \\ &= p(n_0|z_0)p(\theta_0|z_0) \prod_{s=1}^{t} \frac{p(z_s|n_s, \theta_s)\delta(n_s - n_{s-1})p(\theta_s|\theta_{s-1})}{p(z_s|z_{0:s-1})}. \end{aligned} \tag{5}$$

Therefore, by marginalizing over $\theta_{0:t}$ and $n_{0:t-1}$, we obtain

$$p(n_t = l|z_{0:t}) = p(l|z_0) \int_{\theta_0} \cdots \int_{\theta_t} p(\theta_0|z_0) \prod_{s=1}^{t} \frac{p(z_s|l, \theta_s)p(\theta_s|\theta_{s-1})}{p(z_s|z_{0:s-1})} \mathrm{d}\theta_t \cdots \mathrm{d}\theta_0. \tag{6}$$

Thus $p(n_t = l|z_{0:t})$ is determined by the prior distribution $p(n_0 = l|z_0)$ and the product of the likelihood functions, $\prod_{s=1}^{t} p(z_s|l, \theta_s)$. If a uniform prior is assumed, then $\prod_{s=1}^{t} p(z_s|l, \theta_s)$ is the only determining factor.

In the Appendix A, we show that, under some minor assumptions, the posterior probability for the correct identity l, $p(n_t = l|z_{0:t})$, is lower-bounded by an increasing curve which converges to 1.

To measure the evolving uncertainty remaining in the identity variable as observations accumulate, we use the notion of entropy [25]. In the context of this problem, conditional entropy $H(n_t|z_{0:t})$ is used. However, the knowledge of $p(z_{0:t})$ is needed to compute $H(n_t|z_{0:t})$. We assume that it degenerates to an impulse at the actual observations $\tilde{z}_{0:t}$ since we observe only this particular sequence, i.e., $p(z_{0:t}) = \delta(z_{0:t} - \tilde{z}_{0:t})$. Now,

$$H(n_t|z_{0:t}) = -\sum_{n_t \in \mathcal{N}} p(n_t|\tilde{z}_{0:t}) \log_2 p(n_t|\tilde{z}_{0:t}). \tag{7}$$

Under the assumptions listed in the Appendix A, we expect that $H(n_t|z_{0:t})$ decreases as time proceeds since we start from an equi-probable distribution to a degenerate one.

4. Sequential importance sampling algorithm

Consider a general time series state space model fully determined by (i) the overall state transition probability $p(x_t|x_{t-1})$, (ii) the observation likelihood $p(z_t|x_t)$, and (iii) prior probability $p(x_0|z_0)$ and statistical independence among all noise variables. We wish to compute the posterior probability $p(x_t|z_{0:t})$.

If the model is linear with Gaussian noise, it is analytically solvable by a Kalman filter which essentially propagates the mean and variance of a Gaussian distribution over time. For non-linear and non-Gaussian cases, an extended Kalman filter (EKF) and its variants have been used to arrive at an approximate analytic solution [26].

Recently, the SIS technique, a special case of Monte Carlo method, [1,14–16] has been used to provide a numerical solution and propagate an arbitrary distribution over time.

4.1. Importance sampling

The essence of Monte Carlo method is to represent an arbitrary probability distribution $\pi(x)$ closely by a set of discrete samples. It is ideal to draw i.i.d. samples $\{x^{(m)}\}_{m=1}^{M}$ from $\pi(x)$. However it is often difficult to implement, especially for non-trivial distributions. Instead, a set of samples $\{x^{(m)}\}_{m=1}^{M}$ is drawn from an *importance function* $g(x)$ which is easy to sample from, then a weight

$$w^{(m)} = \pi(x^{(m)})/g(x^{(m)}) \tag{8}$$

is assigned to each sample. This technique is called *Importance Sampling* (IS). It can be shown [15] that the *importance sample set* $\mathcal{S} = \{(x^{(m)}, w^{(m)})\}_{m=1}^{M}$ is *properly weighted* to the target distribution $\pi(x)$. To accommodate a video, importance sampling is used in a sequential fashion, which leads to SIS. SIS propagates $\mathcal{S}_{t-1}$ according to the *sequential importance function*, say $g(x_t|x_{t-1})$, and calculates the weight using

$$w_t = w_{t-1}p(z_t|x_t)p(x_t|x_{t-1})/g(x_t|x_{t-1}). \tag{9}$$

In the CONDENSATION algorithm [1], $g(x_t|x_{t-1})$ is taken to be $p(x_t|x_{t-1})$ and Eq. (9) becomes

$$w_t = w_{t-1}p(z_t|x_t), \tag{10}$$

In fact, Eq. (10) is implemented by first resampling the sample set $\mathcal{S}_{t-1}$ according to w_{t-1} and then updating the weight w_t using $p(z_t|x_t)$. For a complete description of the SIS method, refer to [15,16].

The following two propositions are useful for guiding the development of SIS algorithm.

Proposition 1. *When $\pi(x)$ is a PMF defined on a finite sample space, the proper sample set should exactly include all samples in the sample space.*

Proposition 2. *If a set of weighted random samples $\{(x^{(m)}, y^{(m)}, w^{(m)})\}_{m=1}^{M}$ is proper with respect to $\pi(x,y)$, then a new set of weighted random samples $\{(y'^{(k)}, w'^{(k)})\}_{k=1}^{K}$, which is proper with respect to $\pi(y)$, the marginal of $\pi(x,y)$, can be constructed as follows*:

1. *Remove the repetitive samples from $\{y^{(m)}\}_{m=1}^{M}$ to obtain $\{y'^{(k)}\}_{k=1}^{K}$, where all $y'^{(k)}$'s are distinct*;
2. *Sum the weight $w^{(m)}$ belonging to the same sample $y'^{(k)}$ to obtain the weight $w'^{(k)}$, i.e.*,

$$w'^{(k)} = \sum_{m=1, y^{(m)}=y'^{(k)}}^{M} w^{(m)}. \tag{11}$$

4.2. Algorithms and computational efficiency

In the context of this framework, the posterior probability $p(n_t, \theta_t|z_{0:t})$ is represented by a set of *indexed and weighted* samples

$$\mathcal{S}_t = \{(n_t^{(m)}, \theta_t^{(m)}, w_t^{(m)})\}_{m=1}^{M} \tag{12}$$

with n_t as the above index. By Proposition 2, we can sum the weights of the samples belonging to the same index n_t to obtain a proper sample set $\{n_t, \beta_{n_t}\}_{n_t=1}^{N}$ with respect to the posterior PMF $p(n_t|z_{0:t})$.

A straightforward implementation of the CONDENSATION algorithm (Fig. 1) for simultaneous tracking and recognition is not efficient in terms of its computational load. Since $\mathcal{N} = \{1, 2, \ldots, N\}$ is a countable sample space, we need N samples for the identity variable n_t according to Proposition 1. Assume that, for each identity variable n_t, J samples are needed to represent θ_t. Hence, we need $M = J * N$ samples in total. Further assume that one resampling step takes T_r seconds (s), one predicting step $T_p s$, computing one transformed image $T_t s$, evaluating likelihood once $T_l s$. Obviously, the bulk of computation is $J * N * (T_r + T_p + T_t + T_l)s$ to deal with one video frame as the computational time for the normalizing step and the marginalizing step is negligible. It is well known that computing the transformed image is much more expensive than other operations, i.e., $T_t \gg \max(T_r, T_p, T_l)$. Therefore, as the number of templates N grows, the computational load increases dramatically.

There are various approaches in the literature to reduce the computational cost of the CONDENSATION algorithm. In [27], random particles are guided by deterministic search. Assumed density filtering approach [28], different from CONDENSATION, is even more efficient. Those approaches are general and do not explicitly

Initialize *a sample set* $\mathcal{S}_0 = \{(n_0^{(m)}, \theta_0^{(m)}, 1)\}_{m=1}^{M}$ *according to prior distributions* $p(n_0|z_0)$ *and* $p(\theta_0|z_0)$.
For $t = 1, 2, \ldots$
  For $m = 1, 2, \ldots, M$
    Resample $\mathcal{S}_{t-1} = \{(n_{t-1}^{(m)}, \theta_{t-1}^{(m)}, w_{t-1}^{(m)})\}_{m=1}^{M}$ *to obtain a new sample* $(n_{t-1}^{'(m)}, \theta_{t-1}^{'(m)}, 1)$.
    Predict *sample by drawing* $(n_t^{(m)}, \theta_t^{(m)})$ *from* $p(n_t|n_{t-1}^{'(m)})$ *and* $p(\theta_t|\theta_{t-1}^{'(m)})$.
    Compute *transformed image* $\mathcal{T}_{\theta_t^{(m)}}\{z_t\}$.
    Update *weight using* $\alpha_t^{(m)} = p(z_t|n_t^{(m)}, \theta_t^{(m)})$.
  End
  Normalize *each weight using* $w_t^{(m)} = \alpha_t^{(m)} / \sum_{m=1}^{M} \alpha_t^{(m)}$.
  Marginalize *over* θ_t *to obtain weight* β_{n_t} *for* n_t.
End

Fig. 1. The CONDENSATION algorithm.

exploit the special structure of the distribution in this setting: a mixed distribution of continuous and discrete variables. To this end, we propose the following algorithm.

As the sample space $\mathcal{N}$ is countable, an exhaustive search of sample space $\mathcal{N}$ is possible. Mathematically, we release the random sampling in the identity variable n_t by constructing samples as follows: for each $\theta_t^{(j)}$,

$$(1, \theta_t^{(j)}, w_{t,1}^{(j)}), (2, \theta_t^{(j)}, w_{t,2}^{(j)}), \ldots, (N, \theta_t^{(j)}, w_{t,N}^{(j)}).$$

We in fact use the following notation for the sample set,

$$\mathcal{S}_t = \{(\theta_t^{(j)}, w_t^{(j)}, w_{t,1}^{(j)}, w_{t,2}^{(j)}, \ldots, w_{t,N}^{(j)})\}_{j=1}^{J}, \tag{13}$$

with $w_t^{(j)} = \sum_{n=1}^{N} w_{t,n}^{(j)}$. The proposed algorithm is summarized in Fig. 2.

The crux of this algorithm lies in that, instead of propagating random samples on both motion vector and identity variable, we can keep the samples on the identity variable fixed and let those on the motion vector be random. Although we propagate only the marginal distribution for motion tracking, we still propagate the joint distribution for recognition purposes.

The bulk of computation of the proposed algorithm is $J * (T_r + T_p + T_t) + J * N * T_l s$, a tremendous improvement over the CONDENSATION when dealing with a large database since the dominant computational time $J * T_t$ does not depend on N.

Initialize *a sample set* $\mathcal{S}_0 = \{(\theta_0^{(j)}, N, 1, ..., 1)\}_{j=1}^{J}$ *according to prior distribution* $p(\theta_0|z_0)$.
For $t = 1, 2, \ldots$
  For $j = 1, 2, \ldots, J$
    Resample $\mathcal{S}_{t-1} = \{(\theta_{t-1}^{(j)}, w_{t-1}^{(j)})\}_{j=1}^{J}$ *to obtain a new sample* $(\theta_{t-1}^{'(j)}, 1, w_{t-1,1}^{'(j)}, \ldots, w_{t-1,N}^{'(j)})$, *where* $w_{t-1,n}^{'(j)} = w_{t-1,n}^{(j)} / w_{t-1}^{(j)}$ *for* $n = 1, 2, \ldots, N$.
    Predict *sample by drawing* $(\theta_t^{(j)})$ *from* $p(\theta_t|\theta_{t-1}^{'(j)})$.
    Compute *transformed image* $\mathcal{T}_{\theta_t^{(j)}}\{z_t\}$.
    For $n = 1, \ldots, N$
      Update *weight using* $\alpha_{t,n}^{(j)} = w_{t-1,n}^{'(j)} * p(z_t|n, \theta_t^{(j)})$.
    End
  End
  Normalize *each weight using* $w_{t,n}^{(j)} = \alpha_{t,n}^{(j)} / \sum_{n=1}^{N} \sum_{j=1}^{J} \alpha_{t,n}^{(j)}$ *and* $w_t^{(j)} = \sum_{n=1}^{N} w_{t,n}^{(j)}$.
  Marginalize *over* θ_t *to obtain weight* β_{n_t} *for* n_t.
End

Fig. 2. The proposed algorithm.

5. Still-to-video based face recognition

In this section we describe the still-to-video scenarios used in our experiments and their practical model choices, followed by a discussion of experiments. Three databases are used in the still-to-video experiments.

Database-0 was collected outside a building. We mounted a video camera on a tripod and requested subjects to walk straight towards the camera in order to simulate typical scenarios in visual surveillance. Database-0 includes one face gallery, and one probe set. The images in the gallery are listed in Fig. 3. The probe contains 12 videos, one for each individual. Fig. 3 gives some frames in a probe video.

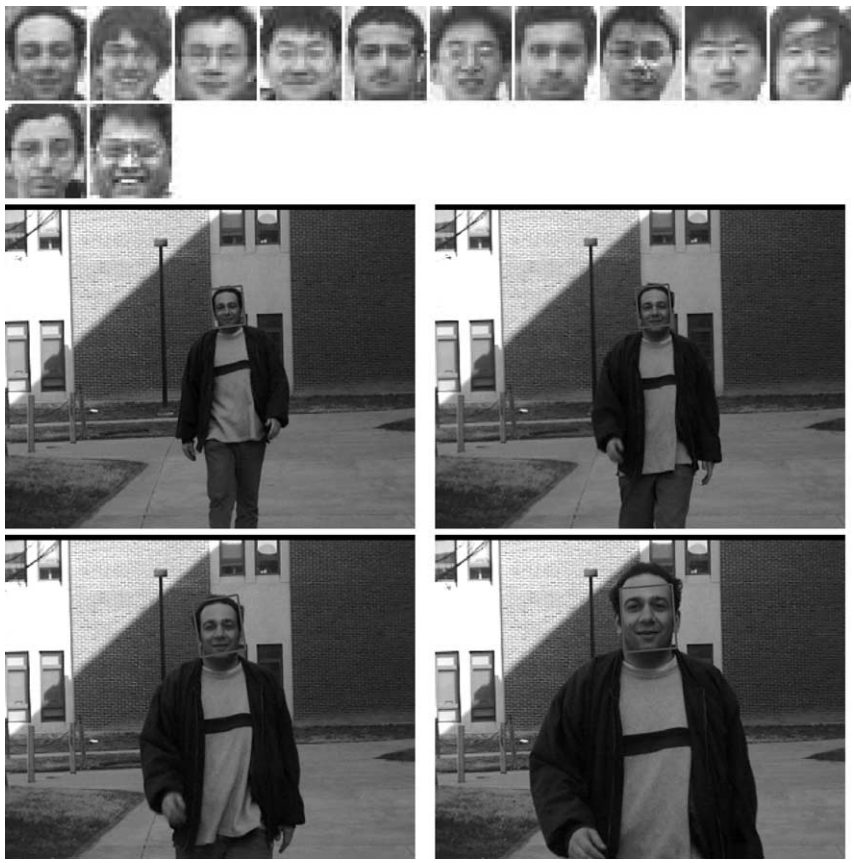

Fig. 3. Database-0. The 1st row: the face gallery with image size being 30×26. The 2nd and 3rd rows: 4 example frames in one probe video with image size being 320×240 while the actual face size ranges approximately from 30×30 in the first frame to 50×50 in the last frame. Notice that the sequence is taken under a well-controlled condition so that there are no illumination or pose variations between the gallery and the probe.

In Database-1, we have video sequences with subjects walking in a slant path towards the camera. There are 30 subjects, each having one face template. There are one face gallery and one probe set. The face gallery is shown in Fig. 4. The probe contains 30 video sequences, one for each subject. Fig. 4 gives some example frames extracted from one probe video. As far as imaging conditions are concerned, the gallery is very different from the probe, especially in lighting. This is similar to the 'FC' test protocol of the FERET test [8]. These images/videos were collected, as part of the HumanID project, by National Institute of Standards and Technology and University of South Florida researchers.

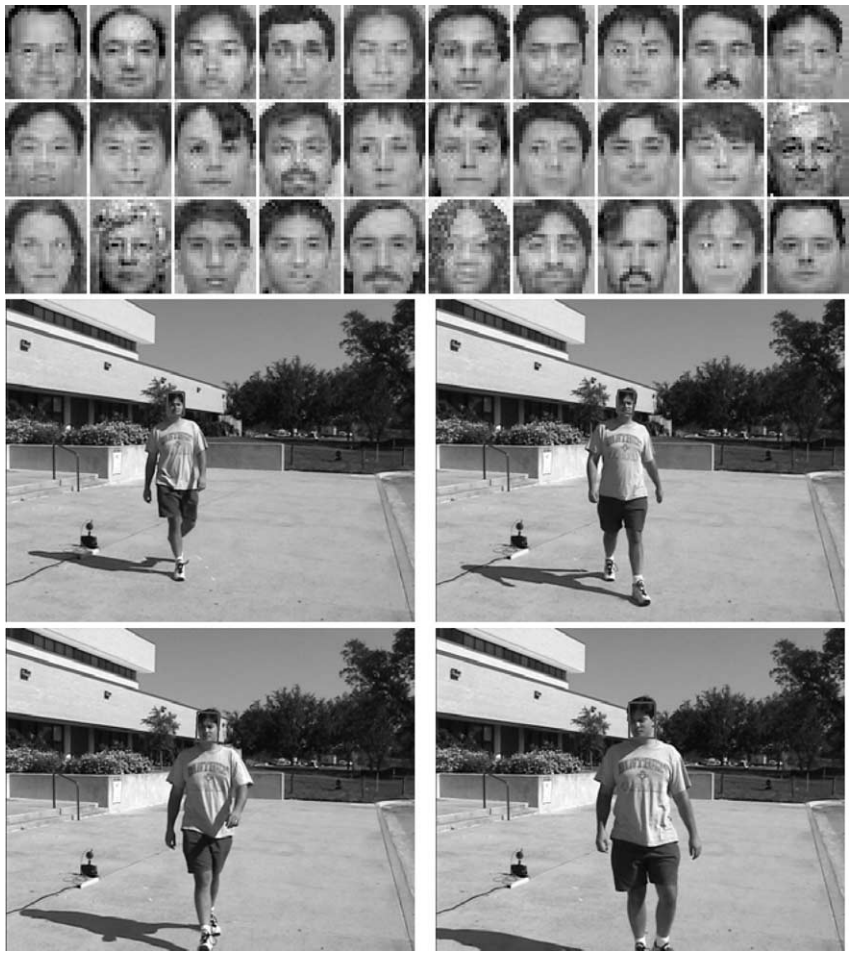

Fig. 4. Database-1. The 1st row: the face gallery with image size being 30×26. The 2nd and 3rd rows: 4 example frames in one probe video with image size being 720×480 while the actual face size ranges approximately from 20×20 in the first frame to 60x60 in the last frame. Notice the significant illumination variations between the probe and the gallery.

Database-2, Motion of Body (MoBo) database, was collected at the Carnegie Mellon University [29] under the HumanID project. There are 25 different individuals in total. The video sequences show the individuals walking on a tread-mill so that they move their heads naturally. Different walking styles have been simulated to assure a variety of conditions that are likely to appear in real life: *walking slowly*, *walking fast*, *inclining*, and *carrying an object*. Therefore, four videos per person and 99 videos in total (with one *carrying* video missing) are available. However, the probe set we use in this section includes only 25 *slowWalk* videos. Some example images of the videos (*slowWalk*) are shown in Fig. 5. Fig. 5 also shows the face gallery in Database-2 with face images in almost frontal view cropped from probe videos and then normalized using their eye positions.

Table 1 summaries the features of the three databases.

5.1. Results for Database-0

We consider affine transformation. Specifically, the motion is characterized by $\theta = (a_1, a_2, a_3, a_4, t_x, t_y)$ where $\{a_1, a_2, a_3, a_4\}$ are deformation parameters and $\{t_x, t_y\}$ are 2D translation parameters. It is a reasonable approximation since there is no significant out-of-plane motion as the subjects walk towards the camera. Regarding the photometric transformation, only zero-mean-unit-variance operator is performed to partially compensate for contrast variations. The complete transformation $\mathcal{T}_\theta\{z\}$ is processed as follows: affine transform z using $\{a_1, a_2, a_3, a_4\}$, crop out the interested region at position $\{t_x, t_y\}$ with the same size as the still template in the gallery, and perform zero-mean-unit-variance operation.

Prior distribution $p(\theta_0|z_0)$ is assumed to be Gaussian, whose mean comes from the initial detector and whose covariance matrix is manually specified.

A time-invariant first-order Markov Gaussian model with constant velocity is used for modeling motion transition. Given the scenario that the subject is walking towards the camera, the scale increases with time. However, under perspective projection, this increase is no longer linear, causing the constant-velocity model to be not optimal. However, experimental results show that as long as the samples of θ can cover the motion, this model is sufficient.

The likelihood measurement is simply set as a 'truncated' Laplacian:

$$p_1(z_t|n_t, \theta_t) = \mathrm{LAP}(\|\mathcal{T}_{\theta_t}\{z_t\} - I_{n_t}\|; \sigma_1, \tau_1), \tag{14}$$

where, $\|\cdot\|$ is sum of absolute distance, σ_1 and λ_1 are manually specified, and

$$\mathrm{LAP}(x; \sigma, \tau) = \begin{cases} \sigma^{-1}\exp(-x/\sigma) & \text{if } x \leqslant \tau\sigma, \\ \sigma^{-1}\exp(-\tau) & \text{otherwise.} \end{cases} \tag{15}$$

Gaussian distribution is widely used as a noise model, accounting for sensor noise, digitization noise, etc. However, given the observation equation: $v_t = \mathcal{T}_{\theta_t}\{z_t\} - I_{n_t}$, the dominant part of v_t becomes the high-frequency residual if θ_t is not proper, and it is well known that the high-frequency residual of natural images is more Laplacian-like. The 'truncated' Laplacian is used to give a 'surviving' chance for samples to accommodate abrupt motion changes.

Fig. 5. Database-2. The 1st row: the face gallery with image size being 30×26. The 2nd and 3rd rows: some example frames in one probe video (*slowWalk*). Each video consists of 300 frames (480×640 pixels per frame) captured at 30 Hz. The inner face regions in these videos contain between 30×30 and 40×40 pixels. Notice the significant pose variation available in the video.

Table 1
Summary of three databases

Database	Database-0	Database-1	Database-2
No. of subjects	12	30	25
Gallery	Frontal face	Frontal face	Frontal face
Motion in probe	Walking straight towards the camera	Walking in an angle towards the camera	Walking on tread-mill
Illumination variation	No	Large	No
Pose variation	No	Slight	Large

Fig. 6 presents the plot of the posterior probability $p(n_t|z_{0:t})$, the conditional entropy $H(n_t|z_{0:t})$ and the minimum mean square error (MMSE) estimate of the scale parameter $sc = \sqrt{(a_1^2 + a_2^2 + a_3^2 + a_4^2)/2}$, all against t. In Fig. 3, the tracked face is superimposed on the image using a bounding box.

Suppose the correct identity for Fig. 3 is l. From Fig. 6, we can easily observe that the posterior probability $p(n_t = l|z_{0:t})$ increases as time proceeds and eventually approaches 1, and all others $p(n_t = j|z_{0:t})$ for $j \neq l$ go to 0. Fig. 6 also plots the decrease in conditional entropy $H(n_t|z_{0:t})$ and the increase in scale parameter, which matches with the scenario of a subject walking towards a camera.

Table 2 summarizes the average recognition performance and computational time of the CONDENSATION and the proposed algorithm when applied to Database-0. Both algorithms achieved 100% recognition rate with top match. The proposed algorithm is much more efficient than the CONDENSATION algorithm. It is more than 10 times faster as shown in Table 1. This experiment was implemented in C++ on a PC with P-III 1G CPU and 512M RAM with the number of motion samples J chosen to be 200, the number of templates in the gallery N to be 12.

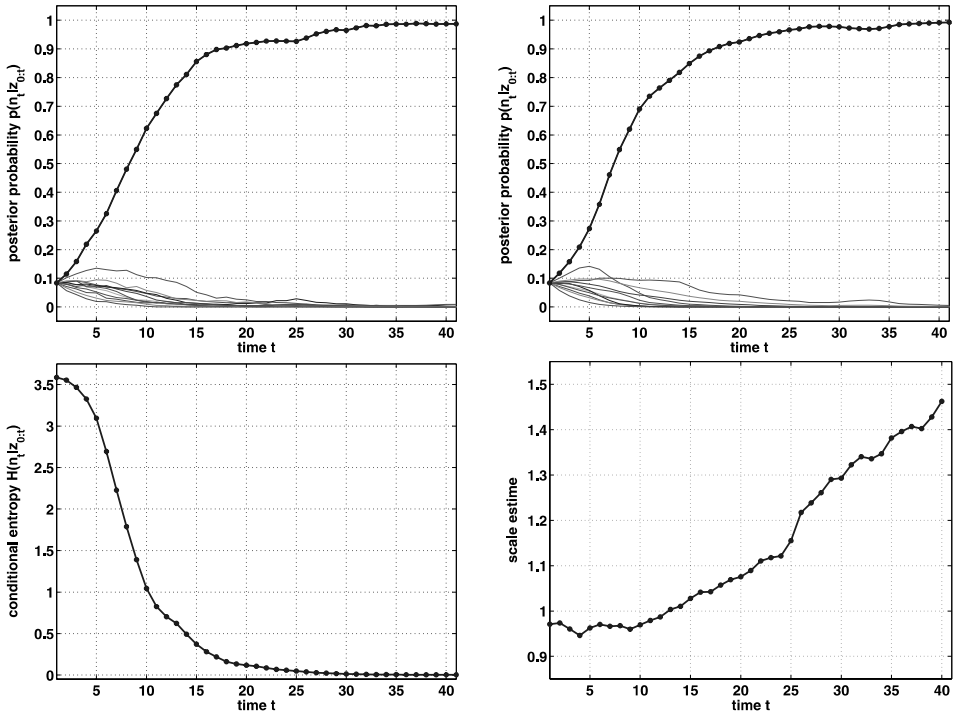

Fig. 6. Posterior probability $p(n_t|z_{0:t})$ against time t, obtained by the CONDENSATION algorithm (top left) and the proposed algorithm (top right). Conditional entropy $H(n_t|z_{0:t})$ (bottom left) and MMSE estimate of scale parameter sc (bottom right) against time t. The conditional entropy and the MMSE estimate are obtained using the proposed algorithm.

Table 2
Recognition performance of algorithms when applied to Database-0

Algorithm	CONDENSATION	Proposed
Recognition rate within top 1 match	100%	100%
Time per frame	7 s	0.5 s

Table 3
Performances of algorithms when applied to Database-1

Case	Case 1	Case 2	Case 3	Case 4	Case 5
Tracking accuracy	83%	87%	93%	100%	NA
Recognition w/in top 1 match	13%	NA	83%	93%	57%
Recognition w/in top 3 matches	43%	NA	97%	100%	83%

5.2. Results on Database-1

Case 1: *Tracking and recognition using Laplacian density*. We first investigate the performance using the same setting as described in Section 5.1. In other words, we still use affine motion parameter, first-order Markov Gaussian state transition model, 'truncated' Laplacian observation likelihood, etc.

Table 3 shows that the recognition rate is very poor, only 13% are correctly identified using top match. The main reason is that the 'truncated' Laplacian density is far from sufficient to capture the appearance difference between the probe and the gallery, thereby indicating a need for a different appearance modeling. Nevertheless, the tracking accuracy[1] is reasonable with 83% successfully tracked because we are using multiple face templates in the gallery to track the specific face in the probe video. After all, faces in both the gallery and the probe belong to the same class of human face and it seems that the appearance change is within the class range.

Case 2: *Pure tracking using Laplacian density*. In Case 2, we measure the appearance change within the probe video as well as the noise in the background. To this end, we introduce a dummy template T_0, a cut version in the first frame of the video. Define the observation likelihood for tracking as

$$q(z_t|\theta_t) = \mathrm{LAP}(\|\mathcal{T}_{\theta_t}\{z_t\} - T_0\|; \sigma_2, \tau_2), \tag{16}$$

where σ_2 and τ_2 are set manually. The other setting, such as motion parameter and model, is the same as in Case 1. We still can run the CONDENSATION algorithm to perform pure tracking.

Table 3 shows that 87% are successfully tracked by this simple tracking model, which implies that the appearance within the video remains similar.

[1] We manually inspect the tracking results by imposing the MMSE motion estimate on the final frame as shown in Figs. 3 and 4 and determine if tracking is successful or not for this sequence. This is done for all sequences and tracking accuracy is defined as the ratio of the number of sequences successfully tracked to the total number of all sequences.

Case 3: *Tracking and recognition using probabilistic subspace density*. As mentioned in Case 1, we need a new appearance model to improve the recognition accuracy. As reviewed in Section 2.1, there are various approaches in the literature. We decided to use the approach suggested by Moghaddam et. al. [18] due to its computational efficiency and high recognition accuracy. However, in our implementation, we model only intra-personal variations instead of both intra/extra-personal variations for simplicity.

We need at least two facial images for one identity to construct the intra-personal space (IPS). Apart from the available gallery, we crop out the second image from the video ensuring no overlap with the frames actually used in probe videos. Fig. 7 (top row) shows a list of such images. Compare with Fig. 4 to see how the illumination varies between the gallery and the probe.

We then fit a probabilistic subspace density [30] on top of the IPS. It proceeds as follows: a regular PCA is performed for the IPS. Suppose the eigensystem for the IPS is $\{(\lambda_i, e_i)\}_{i=1}^{d}$, where d is the number of pixels and $\lambda_1 \geqslant \cdots \geqslant \lambda_d$. Only top s principal components corresponding to top s eigenvalues are then kept while the residual components are considered as isotropic. We refer the reader to the original paper [30]

Fig. 7. Database-1. Top row: the second facial images for training probabilistic density. Middle row: top 10 eigenvectors for the IPS. Bottom row: the facial images cropped out from the largest frontal view.

for full details. Fig. 7 (middle row) show the eigenvectors for the IPS. The density is written as follows:

$$PS(x) = \left\{ \frac{\exp\left(-(1/2)\sum_{i=1}^{s}(y_i^2/\lambda_i)\right)}{(2\pi)^{s/2}\prod_{i=1}^{s}\lambda_i^{1/2}} \right\} \left\{ \frac{\exp\left(-\epsilon^2/2\rho\right)}{(2\pi\rho)^{(d-s)/2}} \right\}, \tag{17}$$

where $y_i = e_i^T x$ for $i = 1, \ldots, s$ is the ith principal component of x, $\epsilon^2 = \|x\|^2 - \sum_{i=1}^{s} y_i^2$ is the reconstruction error, and $\rho = (\sum_{i=s+1}^{d} \lambda_i)/(d-q)$. It is easy to write the likelihood as follows:

$$p_2(z_t|n_t, \theta_t) = PS(\mathcal{T}_{\theta_t}\{z_t\} - I_{n_t}). \tag{18}$$

Table 3 lists the performance by using this new likelihood measurement. It turns out that the performance is significantly better that in Case 1, with 93% tracked successfully and 83% recognized within top 1 match. If we consider the top 3 matches, 97% are correctly identified.

Case 4: *Tracking and recognition using combined density*. In Case 2, we have studied appearance changes within a video sequence. In Case 3, we have studied the appearance change between the gallery and the probe. In Case 4, we attempt to take advantage of both cases by introducing a combined likelihood defined as follows:

$$p_3(z_t|n_t, \theta_t) = p_2(z_t|n_t, \theta_t) q(z_t|\theta_t). \tag{19}$$

Again, all other setting is the same as in Case 1. We now obtain the best performance so far: no tracking error, 93% are correctly recognized as the first match, and no error in recognition when top 3 matches are considered.

Case 5: *Still-to-still face recognition*. To make a comparison, we also performed an experiment on still-to-still face recognition. We selected the probe video frames with the best frontal face view (i.e., biggest frontal view) and cropped out the facial region by normalizing with respect to the eye coordinates manually specified. This collection of images is shown in Fig. 7 (bottom row) and it is fed as probes into a still-to-still face recognition system with the learned probabilistic subspace as in Case 3. It turns out that the recognition result is 57% correct for the top one match, and 83% for the top 3 matches. The cumulative match curves for Case 1 and Cases 3–5 are presented in Fig. 8. Clearly, Case 4 is the best among all. We also implemented the original algorithm by Moghaddam et al. [30], i.e., both intra/extra-personal variations are considered, the recognition rate is similar to that obtained in Case 5.

5.3. Results on Database-2

The recognition result for Database-2 is presented in Fig. 8, using the cumulative match curve. We still use the same setting as in Case 1 of Section 5.2. However, due to the pose variations present in the database, using one frontal view is not sufficient to represent all the appearances under different poses and the recognition rate is hence not so high, 56% when only the top match is considered and 88% when top 3 matches are considered. We do not use probabilistic subspace modeling for this

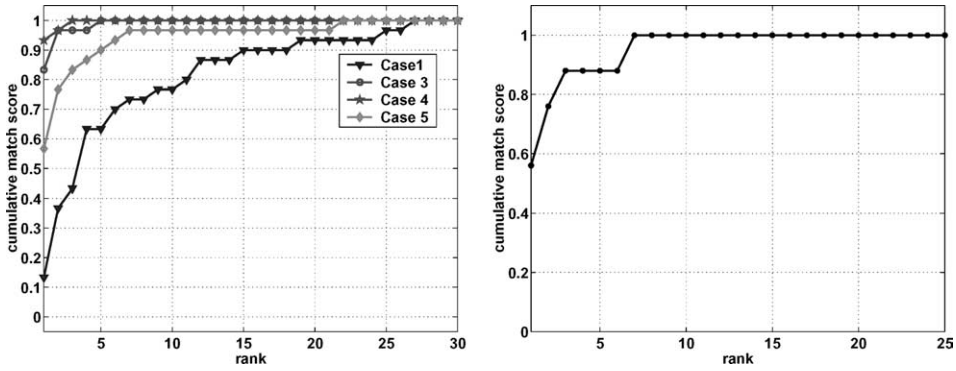

Fig. 8. Cumulative match curves for Database-1 (left) and Database-2 (right).

database because such modeling requires manually cropping out multiple templates for each individual. Also, pre-selecting video frames from the same probe video and ensuring that they do not overlap with the probe frames is time-consuming. What is desirable is to automatically select such templates from different sources other than the probe video. Since we have multiple videos available for one individual in Database-2, this motivates us to obtain more representative views for one face class, leading to the discussions in the next section.

6. Video-to-video based face recognition

In this section we introduce a *video-to-video* based face recognition approach. It enhances the *still-to-video* approach by taking an entire video, instead of a single image, to represent the face of an individual. The *video-to-video* based approach has two stages: In the learning stage, *Exemplars*, which are selected representatives from the raw video, are automatically extracted from gallery videos. The exemplars are used to summarize the gallery video information. In the recognition stage, exemplars are then used as centers for probabilistic mixture distributions for tracking and recognition processes. Probabilistic methods are attractive in this context as they allow a systematic handling of uncertainty and an elegant way for fusing temporal information.

In Section 6.1 we present the learning stage and explain, how the exemplars are generated from a gallery video. In Section 6.2 we explain how tracking and recognition steps are implemented. In Section 6.3 we present experimental results on 99 video sequences of 25 individuals in Database-2.

6.1. Exemplar-based learning

In order to realize *video-to-video* recognition, a probabilistic model needs to be learned from each gallery video V. Denote the gallery as $\mathcal{V} = \{V_1, V_2, \ldots, V_N\}$.

For this, we take an approach which is similar to the ones proposed in [31,32]. These two approaches try to find a set of exemplars that describe the set of training images best, i.e., that minimize the expected distance between the given set of images $\mathcal{Z} = \{z_1, z_2, \ldots, z_J\}$ and a set of exemplars (cluster centers) $\mathcal{C} = \{c_1, c_2, \ldots, c_K\}$.

In other words, let $\mathcal{Z} = \{z_1, z_2, \ldots, z_J\}$ again be the sequence of video images. It is being searched for a set of exemplars $\mathcal{C} = \{c_1, c_2, \ldots, c_K\}$ such that

$$p(z_t) = \sum_{c \in \mathcal{C}} \int_{\Theta} p(z_t|\theta, c) p(\theta|c) p(c) \mathrm{d}\theta \tag{20}$$

is maximal for all t. Here, $p(z_t|\theta, c)$ is the observation equation, given as

$$p(z_t|x) \equiv p(z_t|\theta, c) \propto \exp\left[-\frac{1}{2\sigma^2} d(\mathcal{T}_\theta\{z_t\}, c) \right], \tag{21}$$

where the choice of σ depends on the choice of d, with d being a distance measure.

In [31], the K-means clustering technique is applied to minimize Eq. (20), and in [32] the EM approach is used. The application of the EM approach has drawbacks that were already pointed out by [31]. The application of a K-means clustering technique, as proposed in [31] has, however, the following drawbacks:

- K has to be given in advance. For face recognition this drawback is restrictive: Clearly, the distance measure d may be chosen arbitrarily and for face recognition it is preferable to choose one of the well known ones (e.g., PCA, bunch graph) [8]. Thresholds and variances for each of these measures that minimize mis-classification are known and considering them requires a dynamic choice of the number of clusters rather than a static one.
- Storing the training data in order to compute the clusters becomes computationally intensive for long video streams.

We therefore propose an online technique to learn the exemplars which was inspired by the probabilistic interpretation of the RBF neural network [33]: At each time step t, $p(z_t|\theta, c)$ of Eq. (20) is maximized. If $p(z_t|\theta, c) < \rho$ for some ρ (which depends on the choice of d) then $\mathcal{T}_\theta\{z_t\}$ is added to the set of exemplars.

The details of the learning algorithm are as follows.

1. The first step is the alignment or tracking: a cluster k and a deformation $\theta \in \Theta$ is found such that $d(\mathcal{T}_\theta\{z_t\}, c_k)$ is minimized:

$$\theta_t \leftarrow \arg \min_{\theta} \min_{\mathrm{k}} \mathrm{d}(\mathcal{T}_\theta\{\mathrm{z_t}\}, \mathrm{c_k}) \text{ and } \mathrm{k_t} \leftarrow \arg\min_{\mathrm{k}} \mathrm{d}(\mathcal{T}_{\theta_\mathrm{t}}\{\mathrm{z_t}\}, \mathrm{c_k}). \tag{22}$$

2. The second step generates a new cluster center, if necessary: if

$$p(z_t|\theta_t, c_{k_t}) < \rho$$

then

$$\mathcal{C} \leftarrow \mathcal{C} \cup \{\mathcal{T}_{\theta_t}\{z_t\}\}.$$

Count the number of times, $\mathrm{count}(k_t) = \mathrm{count}(k_t) + 1$, that cluster c_{k_t} approximates image z_t best.

3. Repeat steps one and two until all the frames in the video are processed.

4. Compute the mixture weights $\mu_k \propto \text{count}(k)$.

The result of this learning procedure is

1. A set $\mathcal{C} = \{c_1, c_2, \ldots, c_K\}$ of aligned exemplars c_k.
2. A prior μ_k for each of the exemplars c_k.

Clearly, the more careful the set Θ is chosen, the fewer exemplars are generated. Allowing Θ, e.g., to compensate only for translations, exemplars are generated to compensate scale changes and rotation.

Given a gallery $\mathcal{V}$ of videos, the above has to be carried out for each video. During recognition, as will be explained in the next section, the exemplars are used as centers of mixture models.

The above learning algorithm is motivated by the online learning approaches for artificial neural networks (ANNs) [34,35] and clearly, many enhancements can be attempted (topology preserving maps, neighborhood relations, etc.). An online learning algorithm for exemplars used during testing could allow, in a bootstrapping manner, to learn new exemplars from probe videos.

In [22] a similar learning approach was presented. Contrary to our work, face images are not normalized with respect to Θ which results in a far larger number of clusters. In [20] a 'Unit Face' RBF model is proposed where for each individual, a single RBF network is trained. The authors have also investigated different geometrical normalizations and have experimented with a preprocessing step, such as the application of a 'difference of Gaussians' or Gabor wavelets.

The goal of both of these works was to build a representation of a face intensity by using an RBF network. We want to make clear, that this is exactly what we do not want! Our intention is, to chose a well-known face representation in *advance* (such as, e.g., PCA). *Then*, we learn the different exemplars of a single face. The advantage is that this way we inherit the "face recognition capabilities" of PCA, LDA techniques.

6.2. Tracking and recognition with multiple exemplars

After the application of the learning algorithm we have for each individual n a set of exemplars $\mathcal{C}^n = \{c_1^n, c_2^n, \ldots, c_{K_n}^n\}$. In order to recognize individuals with multiple exemplars, the SIS-approach has to be developed further.

6.2.1. Exemplars as mixture centers

To take into account a set of exemplars $\mathcal{C}^n = \{c_1^n, c_2^n, \ldots, c_{K_n}^n\}$ for individual n, we refine the likelihood computation of Eq. (21) as follows:

$$\begin{aligned} p(z_t|x) &\equiv p(z_t|n,\theta) \\ &\propto \sum_{c\in\mathcal{C}^n} p(z_t|\theta,c)p^n(c) \qquad (23) \\ &\propto \sum_{c\in\mathcal{C}^n} \exp\left[-\frac{1}{2\sigma^2} d(\mathcal{T}_\theta\{z\},c)\right]\mu_c^n. \qquad (24) \end{aligned}$$

The *exemplars* in $\mathcal{C}^{n_t}$ are used as the mixture center of a joint distribution and $p^{n_t}(c) = \mu_c^{n_t}$ is the prior for mixture center c of individual n_t.

6.2.2. Dynamic model

In Section 5, a dynamic model for Eq. (1) has to be given in advance. However, while learning exemplars from video sequences, a dynamic model can also be learned. In Eq. (4)

$$p(x_t|x_{t-1}) \equiv p(\theta_t, n_t|\theta_{t-1}, n_{t-1})$$

defines the probability of the state variable to change from x_{t-1} to x_t. Discussions on learning the dynamic model may be founded in [36,31].

6.2.3. Computation of posterior distribution

The posterior probability distribution $p(n_t, k_t, \theta_t|z_{0:t})$ (where n refers to the individual and k to the exemplar index) is represented by a set of M indexed and weighted particles

$$\left\{\left(n^{(m)}, k^{(m)}, \theta^{(m)}, w^{(m)}\right)\right\}_{m=1,\ldots,M}^{t}. \tag{25}$$

Note that we have, for better readability, indexed the entire set with t, instead of each component. Since all exemplars per person are aligned, we do not have to treat the different exemplars for a single person separately. We can therefore increase efficiency if we rewrite (25) as:

$$\left\{\begin{bmatrix} n^{(m)}, 1, \theta^{(m)}, w_1^{(m)} \\ \vdots \\ n^{(m)}, K_{n^{(m)}}, \theta^{(m)}, w_{K_{n^{(m)}}}^{(m)} \end{bmatrix}\right\}_{m=1,\ldots,M'}^{t}. \tag{26}$$

Set (26) is a set of $K_{n^{(m)}} \times 4$ dimensional matrices, and each matrix represents one particle, where $K_{n^{(m)}} = |\mathcal{C}^{n^{(m)}}|$. We can now easily marginalize over $\mathcal{C}^{n^{(m)}}$ to compute the posterior probability $p(n_t, \theta_t|z_{0:t})$: We get with

$$\hat{w}^{(m)} = \sum_{k=1}^{K_{n^{(m)}}} \mu_k^{n^{(m)}} w_k^{(m)} \tag{27}$$

a new set of weighted sample vectors:

$$\left\{\left(n^{(m)}, \theta^{(m)}, \hat{w}^{(m)}\right)\right\}_{m=1,\ldots,M'}^{t}. \tag{28}$$

In Eq. (27), $\mu_k^{n^{(m)}}$ is the prior of exemplar k of person $n^{(m)}$.

To compute the identity from the particle set (28) we marginalize over θ as in Eq. (11).

6.3. Experimental results

We have tested the *video-to-video* based recognition algorithm on 99 video sequences of 25 different individuals in Database-2. As mentioned before, there are

four walking styles: *walking slowly*, *walking fast*, *inclining*, and *carrying an object*. Therefore, four videos per person are available. In the experiments we used one or two of the video types as gallery videos for training while the remaining ones were used as probes for testing.

For each gallery video, a first face sample was cropped by hand. Based on this sample, the training process was initiated. Four examples of automatically extracted exemplar sets are shown in Fig. 9 (extracted from the videos *slowWalk*). The top row shows the exemplars of subjects 04006 and 04079 (six exemplars each). The leftmost exemplars of each of the two sets are the hand-extracted ones. The 2nd and 3rd rows of Fig. 9 shows the exemplars of subject 04015, and the 4th and 5th rows the exemplars of subject 04022. The top left exemplars of each of the two sets are again the hand-extracted ones. Clearly, the number of generated exemplars depends on the variety of different views that are apparent in the gallery video. To generate these exemplars, we set $\rho = 0.65$ and standard deviation per pixel to $\sigma = 0.4$. Increase of σ to $\sigma = 0.5$ roughly decreased the number of exemplars by a factor of two.

During testing, these exemplar galleries were used to compute, over time, the posterior probabilities $p(n_t|z_{0:t})$. It is interesting to see, how the posterior probabilities develop over time. Examples for this can be seen in Fig. 10. The dash line

Fig. 9. The figure shows exemplars of different persons in gallery videos. In this example, *slowWalk*-videos were used as gallery videos.

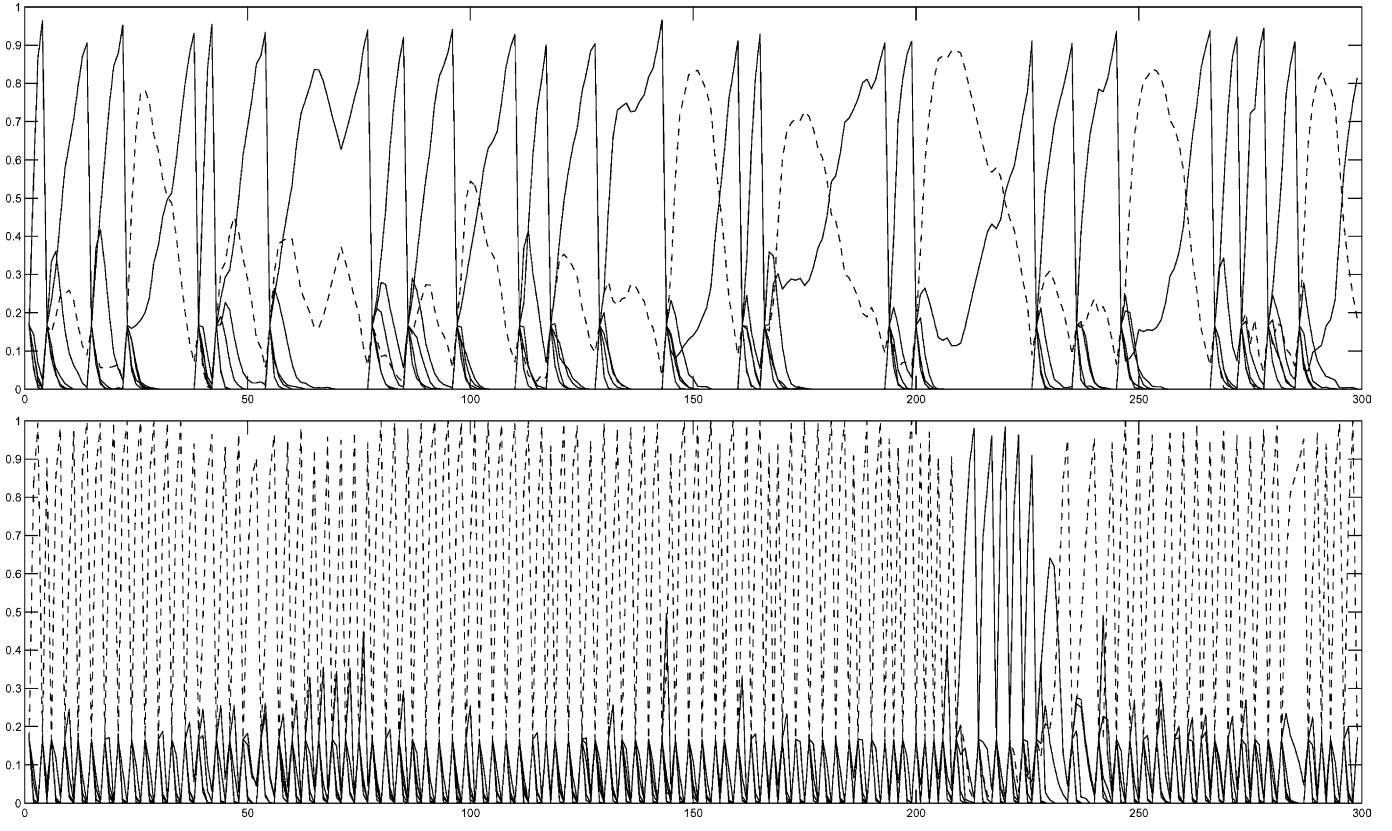

Fig. 10. The figure shows two typical probability evolution. The top row was an unsuccessful recognition, and the bottom row was a successful one. The graphs plot the top 5 matches, the dash line refers to the true hypothesis. The x-axis refers to the time t. The top graph shows the curve of subject 04022, the bottom graph shows a typical curve (here, subject 04079). Compare the top graph with the image in Fig. 11.

refers to the correct hypothesized identity, the other five curves refer to the probabilities of the top matching identities other than the true one. One can see in the left and the right plots that the dash line (true hypothesis) increases quickly to one. In order to consider *all* the frames of the video, we restart the algorithm after convergence. Recognition is established by that identity, to which the SIS converges most often.

Examples illustrating the robustness as well as of the limits of our approach are shown in Figs. 9–12: Due to the severe differences between the gallery exemplars (derived from "slowWalk") in Fig. 9 (4th and 5th row) and the probe video (see sample images from the probe video in Fig. 11), the recognition of subject 04022 was not

Fig. 11. The figure shows sample frames 1, 35, 81, and 100 of a probe video. One observes large differences from the gallery. In this case recognition was *not* successful.

Fig. 12. The figure shows sample frames 1, 9, 40, and 72 of a probe video. One observes large differences from the gallery. In this case, however, recognition *was* successful.

Fig. 13. Images show failure examples, where the galleries were not sufficient to recognize the subjects.

successful (Fig. 10, top). On the other hand, in spite of the differences between the gallery exemplars and the probe video, subject 04079 was always recognized successfully (Fig. 10, bottom).

The major problems that we encountered during our experiments are:

1. Subjects appear significantly different in the gallery video and in the probe videos: This was the case for about 50% of the failed experiments.
2. Subjects looked down while walking: This was the case for roughly 10 subjects (Fig. 13). In some cases, where the subject looked down in the gallery as well as in the probe, this was not a problem. However, in cases, where this happened in only either the probe or the gallery (see Fig. 13, left), this led to mis-classification.

Clearly, both problems can be solved by using more gallery videos. We have therefore done a second set of experiments, where two videos were used as a gallery video, while testing was carried out on the remaining two videos. The overall recognition results for one and two gallery videos are summarized in Table 4. The 'g' indicates, which videos were used in the gallery. The gallery contained 25 different individuals, however, for the "carrying" video set, only 24 different individuals were available.

In [31,36] it is demonstrated that the dynamic information can also be learned. We have done extensive experiments to combine facial and dynamic information

Table 4
Overall recognition rates in percent for $\sigma = 0.4$ and $\sigma = 0.5$

Slow	Fast	Incline	Carrying
For $\sigma = 0.4$			
g	100%	96%	92%
92%	g	100%	96%
100%	96%	g	96%
88%	96%	92%	g
g	g	100%	96%
g	100%	g	100%
g	100%	96%	g
100%	g	g	96%
100%	g	100%	g
100%	100%	g	g
For $\sigma = 0.5$			
g	96%	92%	88%
92%	g	92%	92%
96%	96%	g	96%
88%	88%	83%	g
g	g	96%	92%
g	100%	g	100%
g	96%	96%	g
100%	g	g	96%
92%	g	96%	g
100%	96%	g	g

The 'g' indicates the video used as gallery.

for recognition. However, we have observed, that the dynamic information of persons can change severely with walking speed. Therefore, we have not included that information for recognition.

Video images from our test data were converted from color to gray value images, but no further processing was done. We used throughout our experiments the Euclidean distance measure. The set of deformations Θ included scale and translation. Shear and rotation were not considered.

7. Discussions and conclusions

We have presented a systematic method for face recognition from a probe video, compared with a gallery of still templates. A time series state space model is used to accommodate the video and SIS algorithms provide the numerical solutions to the model. This probabilistic framework, which overcomes many difficulties arising in conventional recognition approaches using video, is registration-free and poses no need for selecting good frames. It turns out that an immediate recognition decision can be made in our framework due to the degeneracy of the posterior probability of the identity variable. The conditional entropy can also serve as a good indication for the convergence. In addition, the still templates in the gallery is generalized to videos by learning exemplars from the gallery video. However, in order to show that our approach is capable of recognizing faces in practice, one needs to work with much larger face databases.

The following issues are worthy of investigation in the future.

1. *Robustness*. Generally speaking, our approach is more robust than still-image-based approach since we essentially compute the recognition score based on all video frames and, in each frame, all kinds of transformed versions of the face part corresponding to the sample configurations that are considered. However, since we take no explicit measure when handling frames with outlier or other unexpected factors, recognition scores based on those frames might be low. But, this is a problem for other approaches too. The assumption that the identity does not change as time proceeds, i.e., $p(n_t|n_{t-1}) = \delta(n_t - n_{t-1})$, could be relaxed by having non-zero transition probabilities between different identity variables. Using non-zero transition probabilities will enable us an easier transition to the correct choice in case that the initial choice is incorrectly chosen, making the algorithm more robust.

2. *Resampling*. In the recognition algorithm, the marginal distribution $\{(\theta_{t-1}^{(j)}, w_{t-1}^{\prime(j)})\}_{j=1}^{J}$ is sampled to obtain the sample set $\{(\theta_t^{(j)}, 1)\}_{j=1}^{J}$. This may cause problems in principle since there is no conditional independence between θ_t and n_t given $z_{0:t}$. However, in a practical sense, this is not a big disadvantage because the purpose of resampling is to 'provide chances for the good streams (samples) to amplify themselves and hence rejuvenate the sampler to produce better results for future states as the system evolves' [15]. The resampling scheme can either be simple random sampling with weights (like in CONDENSATION), residual sampling, or local Monte Carlo methods.

3. *Computational load*. As mentioned earlier, two important numbers affecting the computation are J, the number of motion samples, and N, the size of the database. (i) The choice of J is an open question in the statistics literature. In general, larger J produces more accurate results. (ii) The choice of N depends on application. Since a small database is used in this experiment, it is not a big issue here. However, the computational burden may be excessive if N is large. One possibility is to use a continuous parameterized representation, say γ, instead of discrete identity variable n. Now the task reduces to computing $p(\gamma_t, \theta_t|z_{0:t})$. We then can rank the gallery easily using the estimated γ_t.

4. Now we highlight the differences from Li and Chellappa's approach [5]. In [5], basically only the tracking motion vector is parameterized in the state-space model. The identity is involved only in the initialization step to rectify the template onto the first frame of the sequence. However, in our approach both tracking motion vector and identity variables are parameterized in the state-space model, which offers us one more degree of freedom and leads to a different approach for deriving the solution. The SIS technique is used in both approaches to numerically approximate the posterior probability given the observation. Again in [5], it is the posterior probability of motion vector and the verification probability is estimated by marginalizing over a proper region of state space redefined at each time instant. However, we always compute the joint density, i.e., the posterior probability of motion vector and identity variable and the posterior probability of identity variable is just a free estimate by marginalizing over the motion vector. Note that there is no time propagation of verification probability in [5] while we always propagate the joint density. One consequence is that we guarantee that $\sum_{n_t \in \mathcal{N}} p(n_t|z_{0:t}) = 1$, but there is no such guarantee in [5].

Acknowledgments

We thank the three anonymous reviewers for their critical remarks and valuable suggestions which have considerably improved our paper. The first author would also like to thank Dr. Baback Moghaddam for helpful discussions.

Appendix A. Derivation of the lower bound for the posterior probability of identity

Suppose that the following two assumptions hold:

- (A) The prior probability for each identity is same,

$$p(n_0 = j|z_0) = 1/N;\ j \in \mathcal{N}, \tag{A.1}$$

- (B) for the correct identity $l \in \mathcal{N}$, there exists a constant $\eta > 1$ such that,

$$p(z_t|n_t = l, \theta_t) \geqslant \eta p(z_t|n_t = j, \theta_t);\ t \geqslant 1,\ \ j \in \mathcal{N},\ \ j \neq l. \tag{A.2}$$

Substitution of Eqs. (A.1) and (A.2) into Eq. (6) gives rise to

$$
\begin{aligned}
p(n_t = l|z_{0:t}) &= \frac{1}{N}\int_{\theta_0}\cdots\int_{\theta_t} p(\theta_0|z_0)\prod_{s=1}^{t}\frac{p(z_s|n_s = l,\theta_s)p(\theta_s|\theta_{s-1})}{p(z_s|z_{0:s-1})}\mathrm{d}\theta_t\cdots\mathrm{d}\theta_0\\
&\geqslant \frac{1}{N}\int_{\theta_0}\cdots\int_{\theta_t} p(\theta_0|z_0)\prod_{s=1}^{t}\frac{\eta p(z_s|n_s = j,\theta_s)p(\theta_s|\theta_{s-1})}{p(z_s|z_{0:s-1})}\mathrm{d}\theta_t\cdots\mathrm{d}\theta_0\\
&= \frac{\eta^t}{N}\int_{\theta_0}\cdots\int_{\theta_t} p(\theta_0|z_0)\prod_{s=1}^{t}\frac{p(z_s|n_s = j,\theta_s)p(\theta_s|\theta_{s-1})}{p(z_s|z_{0:s-1})}\mathrm{d}\theta_t\cdots\mathrm{d}\theta_0\\
&= \eta^t p(n_t = j|z_{0:t});\quad j\in\mathcal{N},\ j\neq l,
\end{aligned}
\tag{A.3}
$$

where $\eta^t = \prod_{s=1}^{t}\eta$.

More interestingly, from Eq. (A.3), we have

$$
(N-1)p(n_t = l|z_{0:t}) \geqslant \eta^t\sum_{j=1,j\neq l}^{N} p(n_t = j|z_{0:t}) = \eta^t(1 - p(n_t = l|z_{0:t})),
\tag{A.4}
$$

i.e.,

$$
p(n_t = l|z_{0:t}) \geqslant h(\eta,t),
\tag{A.5}
$$

where

$$
h(\eta,t) = \frac{\eta^t}{\eta^t + N - 1}.
\tag{A.6}
$$

Eq. (A.5) has two implications.

1. Since the function $h(\eta,t)$ which provides a lower bound for $p(n_t = l|z_{0:t})$ is monotonically increasing against time t, $p(n_t = l|z_{0:t})$ has a probable trend of increase over t, even though not in a monotonic manner.
2. Since $\eta > 1$ and $p(n_t = l|z_{0:t}) \leqslant 1$,

$$
\lim_{t\to\infty} p(n_t = l|z_{0:t}) = 1,
\tag{A.7}
$$

implying that $p(n_t = l|z_{0:t})$ degenerates in the identity l for some sufficiently large t.

However, all these derivations are based on assumptions (A) and (B). Though it is easy to satisfy (A), difficulty arises in practice in order to satisfy (B) for all the frames in the sequence. Fortunately, as we have seen in the experiment in Section 5, numerically this degeneracy is still reached even if (B) is satisfied only for most but not all frames in the sequence.

More on Assumption (B).

A trivial choice of η is the lower bound on the likelihood ratio, i.e.,

$$
\eta = \inf_{t\geqslant 1, j\neq l, \theta_t\in\Theta}\frac{p(z_t|n_t = l,\theta_t)}{p(z_t|n_t = j,\theta_t)}.
\tag{A.8}
$$

This choice is of theoretical interest. In practice, how good is the assumption (B) satisfied? Fig. 14 plots, against the logarithm of the scale parameter, the 'average' likelihood of the correct identity,

$$
\frac{1}{N}\sum_{n\in\mathcal{N}} p(I_n|n,\theta),
$$

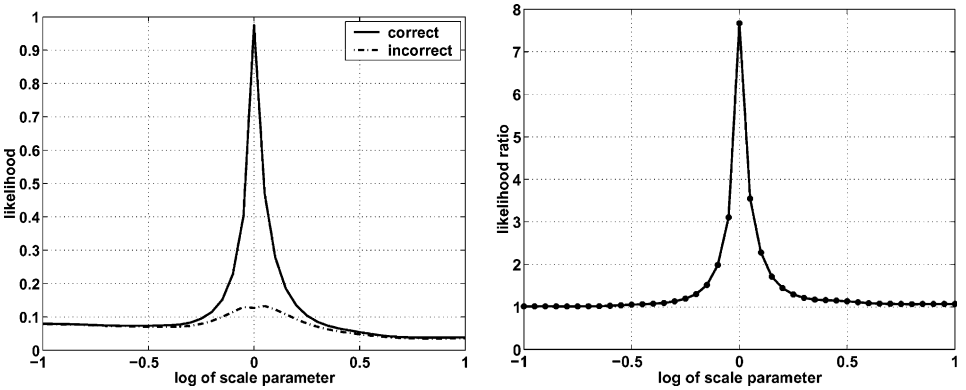

Fig. 14. Left: the 'average' likelihood of the correct hypothesis and incorrect hypotheses against the log of scale parameter. Right: the 'average' likelihood ratio against the log of scale parameter.

and that of the incorrect identities,

$$\frac{1}{N(N-1)} \sum_{m\in\mathcal{N}, n\in\mathcal{N}, m\neq n} p(I_m|n,\theta),$$

of the face gallery as well as the 'average' likelihood ratio, i.e., the ratio between the above two quantities. The observation is that only within a narrow 'band' the condition (B) is well satisfied. Therefore, the success of SIS algorithm depends on how good the samples lie in a similar 'band' in the high-dimensional affine space. Also, the lower bound η in assumption (B) is too strict. If we take the mean of the 'average' likelihood ratio shown in Fig. 14 as an estimate of η (roughly 1.5), Eq. (A.5) tells that, after 20 frames, the probability $p(l|y_{0:t})$ reaches 0.99! However, this is not reached in the experiments due to noise in the observations and incomplete parameterization of transformations.

References

[1] M. Isard, A. Blake, Contour tracking by stochastic propagation of conditional density, Proc. ECCV (1996) 343–356.
[2] N.J. Gordon, D.J. Salmond, A.F.M. Smith, Novel approach to nonlinear/non-gaussian bayesian state estimation, IEE Proc. Radar Signal Process. 140 (1993) 107–113.
[3] M.J. Black, A.D. Jepson, A probabilistic framework for matching temporal trajectories, Proc. ICCV (1999) 176–181.
[4] G. Qian, R. Chellappa, Structure from motion using sequential Monte Carlo methods, Proc. ICCV (2001) 614–621.
[5] B. Li, R. Chellappa, A generic approach to simultaneous tracking and verification in video, IEEE Trans. Image Process. 11 (2002) 530–544.
[6] R. Chellappa, C.L. Wilson, S. Sirohey, Human and machine recognition of faces: a survey, Proc. IEEE 83 (1995) 705–740.

[7] W.Y. Zhao, R. Chellappa, A. Rosenfeld, P.J. Phillips, Face Recognition: A Literature Survey, UMD CfAR Technical Report CAR-TR-948, 2000.
[8] P.J. Philipps, H. Moon, S. Rivzi, P. Ross, The feret evaluation methodology fro face-recognition algorithms, IEEE Trans. PAMI 22 (2000) 1090–1104.
[9] M. Turk, A. Pentland, Eigenfaces for recognition, J. Cognitive Neurosci. 3 (1991) 72–86.
[10] K. Etemad, R. Chellappa, Discriminant analysis for recognition of human face images, J. Opt. Soc. Am. A (1997) 1724–1733.
[11] P.N. Belhumeur, J.P. Hespanha, D.J. Kriegman, Eigenfaces vs. fisherfaces: recognition using class specific linear projection, IEEE Trans. PAMI 19 (1997) 711–720.
[12] M. Lades, J.C. Vorbruggen, J. Buhmann, J. Lange, C. von der Malsburg, R.P. Wurtz, W. Konen, Distortion invariant object recognition in the dynamic link architecture, IEEE Trans. Computers 42 (3) (1993) 300–311.
[13] T. Choudhury, B. Clarkson, T. Jebara, A. Pentland, Multimodal person recognition using unconstrained audio and video, in: Proceedings of International Conference on Audio- and Video-Based Person Authentication, 1999, pp. 176–181.
[14] G. Kitagawa, Monte carlo filter and smoother for non-gaussian nonlinear state space models, J. Comput. Graphical Statistics 5 (1996) 1–25.
[15] J.S. Liu, R. Chen, Sequential Monte Carlo for dynamic systems, J. Am. Statist. Assoc. 93 (1998) 1031–1041.
[16] A. Doucet, S.J. Godsill, C. Andrieu, On sequential Monte Carlo sampling methods for bayesian filtering, Statist. Computing 10 (3) (2000) 197–209.
[17] R.O. Duda, P.E. Hart, D.G. Stork, Pattern Classification, Wiley-Interscience, New York, 2001.
[18] B. Moghaddam, T. Jebara, A. Pentland, Bayesian modeling of facial similarity, Adv. in Neural Information Processing Systems 11 (1999) 910–916.
[19] T. Jebara, A. Pentland, Parameterized structure from motion for 3D adaptive feedback tracking of faces, Proc. CVPR (1997) 144–150.
[20] A. Howell, H. Buxton, Face recognition using radial basis function neural networks, in: Proceedings of the British Machine Vision Conference, 1996, pp. 455–464.
[21] S. McKenna, S. Gong, Non-intrusive person authentication for access control by visual tracking and face recognition, in: Proceedings of the International Conference on Audio- and Video-based Biometric Person Authentication, 1997, pp. 177–183.
[22] H. Wechsler, V. Kakkad, J. Huang, S. Gutta, V. Chen, Automatic video-based person authentication using the RBF network, in: Proceedings of the International Conference on Audio- and Video-based Biometric Person Authentication, 1997, pp. 85–92.
[23] J. Steffens, E. Elagin, H. Neven, Personspotter—fast and robust system for human detection, tracking, and recognition, in: Proceedings of the International Conference on Automatic Face and Gesture Recognition, 1998, pp. 516–521.
[24] Y. Li, S. Gong, H. Liddell, Modelling faces dynamically across views and over time, Proc. ICCV (2001) 554–559.
[25] T.M. Cover, J.A. Thomas, Elements of Information Theory, Wiley, New York, 1991.
[26] B. Anderson, J. Moore, Optimal Filtering, Prentice Hall, Englewood Cliffs, New Jersey, 1979.
[27] J. Sullivan, J. Rittscher, Guiding random particle by deterministic search, Proc. ICCV (2001) 323–330.
[28] X. Boyen, D. Koller, Tractable inference for complex stochastic processes, in: Proceedings of the 14th Annual Conference on Uncertainty in AI (UAI), Madison, WI, 1998 pp. 33–42.
[29] R. Gross, J. Shi, The CMU Motion of Body (MoBo) Database, CMU-RI-TR-01-18, 2001.
[30] B. Moghaddam, Principal manifolds and probabilistic subspaces for visual recognition, IEEE Trans. PAMI 24 (2002) 780–788.
[31] K. Toyama, A. Blake, Probabilistic tracking in a metric space, Proc. ICCV (2001) 50–59.
[32] B. Frey, N. Jojic, Learning graphical models in images, videos, and their spatial transformations, in: Proceedings of the Conference on Uncertainty in AI, 2000, pp. 184–191.
[33] D. Lowe, Radial basis function networks, in: M. Arbib (Ed.), The Handbook of Brain Theory and Neural Networks, 1995, pp. 779–782.

[34] B. Fritzke, Growling cell structures—a self-organizing network for unsupervised and supervised learning, Neural Learning 7 (1995) 1441–1460.
[35] T. Martinez, K. Schulten, Topology representing networks, Neural Learning 7 (1994) 505–522.
[36] B. North, A. Blake, M. Isard, J. Rittscher, Learning and classification of complex dynamics, IEEE Trans. PAMI 22 (2000) 1016–1034.